scientific reports

Check for updates

OPEN

Dictyostelium exhibits PCB-induced impairment of proliferation, development and stress response, emerging as model for conserved environmental toxicity

Simone Rocco, Cristina Panuzzo✉, Valentina Schiavo, Giusi Balsano, Alessandro Ferrando & Barbara Pergolizzi✉

Persistent Organic Pollutants, such as polychlorinated biphenyls (PCBs), are environmental pollutants for their resistance to degradation and adverse health effects. Despite extensive toxicological data in mammalian system, the use of alternative models such as *Dictyostelium discoideum* offers an opportunity to dissect evolutionarily conserved molecular mechanisms underlying pollutant-induced cellular dysfunction. In this study, we used *Dictyostelium* to investigate the effects of PCB 138 and PCB 153 revealing, for the first time, a direct impairment of both growth and multicellular development. PCBs exposure reduced cell proliferation and led to the formation of smaller fruiting bodies. These phenotypic effects were accompanied by altered expression of iron-regulatory genes, including upregulation of *abcb7* and *ferroportin*, and downregulation of *ferritin*, consistent with intracellular iron depletion confirmed by calcein assay. We used THP-1 human cells to confirm the effect of PCBs on *hamp* gene, supporting the relevance of iron homeostasis as a target pathway. In *Dictyostelium*, iron imbalance was associated with increased ROS levels, downregulation of superoxide dismutase genes, and altered mitochondrial morphology. Under starvation, PCBs-treated cells also showed transcriptional upregulation of key development genes involved in cAMP signaling (*acaA*, *carA*, *regA*, *gtaC*), while proteomic analysis revealed changes in proteins linked to cell adhesion, stress response, and development. Together these findings support a model in which PCBs induce iron efflux, oxidative stress, and disruption of developmental signaling, ultimately both proliferation and morphogenesis. This study highlights the potential of *Dictyostelium discoideum* as a sensitive and cost-effective model to uncover conserved cellular responses to environmental pollutants.

Keywords Polychlorinated Biphenyl (PCBs), *Dictyostelium*, HumanTHP1cells, cAMP signalling, Iron homeostasis, Cellular toxicity

Persistent organic pollutants (POPs) are a class of chemicals, primarily of anthropological origin, that persist in the environment. They can be divided into three main subclasses: pesticides (e.g. DDT), industrial chemical-like substances, such as polychlorinated biphenyls (PCBs), and their by-products, like polychlorinated dibenzodioxins (PCDDs)[1]. Due to their chemical structure, POPs can resist degradation and persist for decades, eventually being absorbed by plants and animals. In fact, POPs tend to accumulate in the fatty tissue of living organisms, and their bioaccumulation increases up in the food chain[1]. Consequently, approximately 90% of human exposure to POPs comes from consuming contaminated food, although exposure can also occur through inhalation and direct contact[1–4].

PCBs consist of a biphenyl structure with various numbers of hydrogen and chlorine atoms attached, resulting in 209 different congeners with varying toxicity levels (French Agency for Food, Environmental and Occupational Health & Safety, (ANSES 2011, s. d.). They are classified into dioxin like (DL), and non-dioxin like (NDL). Among the NDL, PCB 138 and PCB 153 both contain six chlorine atoms differing primarily in their position, which affect their chemical and toxicological properties. DL and NDL PCBs have different

Department of Clinical and Biological Sciences, Medical School, University of Torino, 10043 Orbassano, Italy. ✉email: cristina.panuzzo@unito.it; barbara.pergolizzi@unito.it

toxic mechanisms. NDL PCBs interact with multiple cellular receptors and can act as endocrine disruption through diverse molecular pathways, potentially impacting neurodevelopment and behavior[5]. Generally, NDL PCBs act as indirect, non-genotoxic carcinogens, tumor promoters, and their mechanisms include suppression of apoptosis in preneoplastic cells and inhibition of intercellular communication[6]. In 2016, the International Agency for Research on Cancer (IARC) upgraded PCBs from the previous Group 2 A "Probably carcinogenic to humans" to Group 1 "Carcinogenic to humans"[7], primarily based on sufficient evidence showing an increased risk of cutaneous malignant melanoma[1,8].

PCBs have been associated with immune-toxic and pro-inflammatory effects, leading to endocrine, reproductive and neurodevelopmental deficits[9,10]. Importantly, epidemiological studies link PCBs to numerous blood-related adverse health effects, including immunosuppression, macrophage impairment, and hematological diseases such as Childhood Leukemia and Non-Hodgkin's Lymphoma (NHL)[11–13].

At the cellular level, PCBs can induce oxidative stress, primarily through their interaction with the electron transport chain in mitochondria or the activation of NADPH oxidase leading to DNA, lipid, and protein damage[14–17]. In addition, studies have shown that PCBs disrupt the iron homeostasis by suppressing hepcidin (HAMP) expression through estrogen response elements in its promoter[18,19]. Hepcidin is the master regulator of systemic iron balance and maintains iron homeostasis by binding to the iron exporter ferroportin, triggering its internalization and degradation. This process limits iron efflux into the circulation, thereby preventing iron overload in plasma and target tissue. Disruption of this regulatory axis can profoundly affect both cellular and systemic iron metabolism with downstream effects on multiple physiological process[21,22].

Despite these insights, the specific mechanisms linking PCBs and iron metabolism remain still unknown. Understanding these mechanisms can shed light on the broader implications of PCBs exposure on human health and disease progression[22,23]. Further research is required to detail the pathways through which PCBs contribute to the dysregulation of cell cycle life.

To investigate evolutionarily conserved mechanisms of PCB toxicology, we employed *Dictyostelium discoideum* (referred to as *Dictyostelium)*, a non-mammalian model organism recognized by NIH as a model for human health. *Dictyostelium* lives in natural soil habitats, and several studies of wild clones have increasingly focused on understanding the interactions between different isolated clones to gain insights into their evolutionary advantages[24]. Since 1970 s, *Dictyostelium* lab strains were selected to be capable of growing axenically in a mixture of peptone and yeast extract or in defined minimal media due to deletion of several genes, particularly the gene encoding the putative RasGAP NF1 that enhances fluid-phase uptake through macropinocytosis, a process that is highly inefficient or even absent in the parental wild-type isolates[25]. Due to its unique characteristics, *Dictyostelium* is extensively studied for various cellular processes, including phagocytosis, bacterial infection, chemotaxis, cellular migration towards different sources and others[26–28]. Its ability to transition from a unicellular to a multicellular organism makes it an ideal model for investigating how cells move and respond to chemical signals. The studies using *Dictyostelium* have broad implications for understanding fundamental biological processes and diseases in higher organisms. Under favorable conditions, the amoeba feeds on bacteria and divides through binary fission[29–31]. When food became scarce, *Dictyostelium* cells entered a starvation phase, triggering a remarkable transformation: the solitary cells aggregate through chemotaxis in response to cAMP undergoing morphological changes to form a thing finger, which can quickly convert to a slug and migrate for varying periods through phototaxis or thermotaxis[32–34]. Under favorable conditions for sporulation, the slug ceases migration and undergoes culmination, resulting in the mature multicellular organism. This structure, a fruiting body, has 20% of its cells forming a stalk of dead, vacuolated cells that supports a spore head containing 80% of the cells as spores[35].

Dictyostelium was studied for pharmacological research as a valuable model for toxicity assessment of drugs, toxin and other harmful compounds[31,36,37]. It is also being explored as a potential experimental system for evaluating the toxicity of soil exposed to aqueous media contaminated with non-essential heavy metals and organic xenobiotic compounds to evaluate stress responses[38–40].

We selected PCB 138 and PCB 153 because they have been identified in human serum and tissue. Their established association with hematological diseases[13,41], including leukemia, makes them particularly relevant to our study focus, which builds on our previous. Indeed, in recent years, our research has also expanded to explore the role of the ubiquitin system in Chronic Myeloid Leukemia (CML), following our identification of an E3 ubiquitin ligase in *Dictyostelium* that is essential for differentiation, and orthologous to HERC1 in mammals[42–44].

Our analysis focused on PCBs-induced remodeling gene expression related to iron and cAMP signaling, oxidative stress responses, and mitochondrial morphology. A differential proteomic analysis further revealed alterations in the *Dictyostelium* proteome upon exposure to these environmental toxicants. Notably, we investigated, for the first time, how PCB exposure affects cell aggregation and morphogenesis during *Dictyostelium* development. Thanks to its unique life cycle and conserved genome *Dictyostelium* represents a powerful model to dissect the cellular mechanism underlying PCB-induced toxicity. Our findings offer novel insight into conserved molecular targets and may contribute to a better understanding of how PCBs impact human health.

Materials and methods

Dictyostelium and THP-1 cells culture

Dictyostelium Ax4 cells were cultured in suspension in axenic mediu[45] at 23 °C under shaking at 150 rpm in a climatic cabinet equipped with gyratory shakers (Kühner, Bielefeld, Switzerland). Instead, Ax4::Fxn-GFP were selectively grown in presence of 10 µg/ml G418. Electroporation was performed using 10 µg of Fxn-GFP plasmid, following the procedure described by[46].

THP-1 cells (ATCC TIB-202) were grown in suspension in RPMI medium, supplied with 10% FBS and 1% penicillin/streptomycin, in an incubator at 37 °C, 5% CO2.

Axenic growth assay

Ax4 cells were grown and monitored for 3 or 5 days in axenic medium, supplemented with different concentrations of PCB 138 and PCB 153 (Sigma Aldrich, n code: 35,494, 35,602 respectively), which was resuspended in DMSO. The same concentrations of DMSO were added in non-treated (Vehicle) samples as a control. The cells were set at the same initial concentration of 1×10^5 cells/mL and counting them every day at the same hour and the number of generations reached after each day. The experiment was repeated three times and standard deviations were calculated based on the means of each sample. One-way ANOVA with Dunnett's multiple comparisons test was performed with GraphPad Prism 8 (https://www.graphpad.com/) on the 3rd day of count, to check for statistical significance.

Dictyostelium development assay

Cells were centrifuged at 1,000 g for 3 min in an Eppendorf centrifuge, washed twice with *Sörensen* and finally resuspended in the same buffer at a concentration of 1×10^7 cells/mL. Small drops of 20 µL of the suspension were deposited on non-nutrient agar (agar P) where, for treated samples, PCB 138 or PCB 153 were previously added at a concentration of 50 µM. Different pictures were taken with a digital microscope imager (Celestron) at well-established time points, typical of *Dictyostelium* developmental life cycle: 0, 5, 8, 24 and 48 h. To assess pre-exposure effects, cells were also cultured in axenic medium with either PCB138 or PCB153 (50 µM) for 3 days or 5 days. After the treatment period, cells were washed and subjected to the same development assay, this time without PCBs added to the agar. Since the phenotypic outcomes after 5 days of treatment were comparable to those observed at 3 days, we chose to standardize the treatment duration to 3 days, in line with commonly adopted protocols in the *Dictyostelium* research community.

XTT assay

THP-1 cells were treated with PCB 138 or PCB 153 at different concentrations (1 µM, 10 µM, 50 µM and 100 µM) for 3 days. Then, cell vitality was tested using the cell proliferation Kit XTT (Roche, n code: 11,465,015,001), by measuring the changes in absorbance at 450 nm, after 3 h of incubation at 37 °C, 5% CO_2. A total of 2×10^4 cells (in 100 µL of medium) per well were used on the 96-well plate. All conditions were seeded in triplicate. One-way ANOVA with Dunnett's multiple comparisons test was performed with GraphPad Prism 8 (https://www.graphpad.com/) for statistical significance.

RNA isolation and retrotranscription

A total of 1×10^7 Ax4 cells and 1×10^6 THP-1 cells were collected after treatment and resuspended in 500 µL of TRIzol Reagent (Ambion, Thermo Fisher, n code: 15,596,026) to isolate the RNA according to the manufacturer's protocol. RNA concentration was measured at the spectrophotometer and stored at – 80 °C until use. Subsequently, 1 µg of RNA for each sample was retrotranscribed using the SensiFAST cDNA Synthesis kit (Bioline, Meridian Bioscience). Samples were incubated for 10 min at 25 °C, followed by 15 min at 42 °C and 5 min at 85 °C for complete inactivation. cDNA samples were stored at – 20 °C until use.

Real-time PCR (qPCR)

qPCR was performed using the SensiFAST SYBR kit (Bioline, n code: BIO-98005). *Cycloheximide-INducible D1* (*cinD-1*) and *glucuronidase beta* (*gusB*) were used as reference genes for the analysis in *Dictyostelium* and human cells, respectively. The reaction mix for each gene was composed of 5 µL of SYBR Green, 0.2 µL of each primer (10 µM) and 2.1 µL of PCR-grade water. 2.5 µL of cDNA samples were added directly on the 96-well plate. qPCR was performed according to the protocol provided by the company. Results were examined on Bio-Rad CFX Manager 3.1 software (https://www.bio-rad.com/it-it/sku/1845000-cfx-manager-software?ID=1845000) and relative normalized expression was calculated setting NT samples as reference for the analysis. One-way ANOVA with Dunnett's multiple comparisons test was performed with GraphPad Prism 8 (https://www.graphpad.com/) for statistical significance. The complete list of used primers is reported in Table S1.

Confocal analysis of mitochondria and ROS measurement

Ax4::Fxn-GFP cells were treated for 3 days with 50 µM of either PCB 138 or PCB 153. After treatment, cells were deposited on a glass slide and left to adhere for 5 min. The medium was then carefully aspirated to avoid removing adherent cells and replaced with *Sörensen* buffer for an additional 5 min. Live mitochondrial fluorescence was visualized using a Zeiss LSM 510 confocal microscope equipped with a 63X/1.40 immersion oil objective. Z-stacks (0.20 µm thickness) were acquired and merged into a single 2D projection using the ImageJ Z-project plugin. Subsequently, mitochondrial morphology was analyzed using the MiNa plugin[47]. Images were pre-processed through unsharp mask, CLAHE and median filtering, then binarized and eventually skeletonized before the analysis.

ROS levels were measured following the protocol described by[48]. Basically, Ax4 cells were treated with 50 µM of PCB 138 or PCB 153 for 3 days. After treatment, cells were centrifuged at 1,000 g for 3 min and resuspended in *Sörensen* buffer supplied with 0.12 M sorbitol, at a final concentration of 6×10^6 cells/mL. Then, 50 µL of cell suspension were transferred into each well of a black 96-well plate. Subsequently, equal volume (50 µL) of 60 µM dihydroethidium (DHE) was added in each well. Fluorescence (excitation/emission 560 nm/590 nm, ± 20 nm) was recorded every 2 min for 1 h using a Microplate reader Infinite 200 (Tecan), under medium shake (5 s/min) at 23 °C. Three biological replicates were performed, and statistical significance was evaluated by One-way ANOVA with Dunnett's multiple comparisons test with GraphPad Prism 8 (https://www.graphpad.com/).

Western blot

A total of 1×10^7 Ax4 cells were lysed on ice using 100 µL of RIPA buffer (20 mM Tris–HCl pH 7.5, 150 mM NaCl, 0.1% SDS, 1 mM EDTA, 1 mM EGTA and 1% NP-40) supplemented with protease inhibitors (Roche, Sigma Aldrich, n code: 05,892,970,001). Lysates were incubated on ice for 30 min with occasional vortexing and then centrifugated at 13,000 g for 15 min at 4 °C to remove debris. Protein concentration was determined using the Bradford assay, and 30 µg of total protein per sample were load onto a 10% SDS–polyacrylamide gel for electrophoresis. Proteins were separated by SDS-PAGE and transferred onto a PVDF membrane (Millipore) using a wet transfer system at 100 V for 1 h at 4 °C. Membranes were blocked with 5% non-fat dry milk in TBS-T (Tris-buffered saline with 0.3% Tween-20) for 1 h at room temperature and then incubated overnight at 4 °C with polyclonal anti-RegA primary antiserum (kindly provided by the David Traynor lab, *Dictyostelium* research community). After washing, membranes were incubated for 1 h at room temperature with HRP-conjugated anti-rabbit secondary antibody (Santa Cruz Biotechnology).

Signal detection was performed using enhanced chemiluminescence (ECL, Bio-Rad) and images were acquired with the ChemiDoc Touch Imaging System (Bio-Rad). Band intensity analysis was carried out using Image Lab 6.1 software (https://www.bio-rad.com/it-it/product/image-lab-software?ID=KRE6P5E8Z). Three biological replicates were performed, and statistical significance was evaluated by One-way ANOVA with Dunnett's multiple comparisons test with GraphPad Prism 8 (https://www.graphpad.com/).

Calcein fluorescence quenching assay for intracellular iron measurement

After the 3-day treatment with PCB 138 or PCB 153, 2.5×10^5 Ax4 cells were washed twice and resuspended in *Sörensen* buffer at a concentration of 1×10^5 cells/mL. Calcein was then added to the suspension at a final concentration of 5 µM. Cells were incubated for 30 min at 150 rpm, protected by light. Subsequently, cells were washed twice to remove excess dye and resuspended in 500 µL of *Sörensen*. Mean fluorescent signal intensity (MFI) was measured using BD FACS Cell Analyzer instrument (Celesta), to indirectly evaluate intracellular iron levels. Three replicates were performed and data were analyzed using FlowJo 10 software (https://www.flowjo.com/). One-way ANOVA with Dunnett's multiple comparisons test was performed with GraphPad Prism 8 (https://www.graphpad.com/) for statistical significance.

Proteomic analysis

Ax4 cells were cultured in axenic medium for 3 days with PCB 138 (50 µM), washed twice with *Sörensen* and let them starve for 8 h to induce aggregation, following the same methodology described before. A total of 1×10^7 cells were collected in a 1.5 mL tube, centrifuged at 13,000 g for 5 min at 4 °C and finally resuspended in 600 µL of RIPA buffer. Samples were kept on ice for 10 min, then sonicated twice for 10 s (with a 5 s pause between pulses). After a second centrifugation, 300 µL of the total lysate were transferred to a new tube adding 900 µL of acetone and incubated at −20 °C overnight. The day after, the sample was centrifuged again at 13,000 g for 10 min at 4 °C. The supernatant was discarded, the pellet was dried for 30 min and finally resuspended in 100 µL of a specific lysis buffer (8 M urea, 4% CHAPS and Pharmalyte 3–10).

For the first dimension, 150 µg of protein lysate were mixed with 105 µL of RH buffer (7 M urea, 2 M thiourea, 2% CHAPS, 20 mM DTT, 0.5% IPG buffer, 0.02% blue bromophenol and 1.7 µL streaking solution) and incubated for 1 h at room temperature. Samples were then sonicated twice on ice for 10 s (5 s pause between the two pulses) and electro-focused using Ettan IPGphor instrument (GE Healthcare-ThermoFisher) on Immobiline DryStrip (7 cm length, pH range: 3–10 NL; BioRAD), in order to separate the proteins according to their isoelectric point. Once the run was finished, the strips were left in SDS-equilibration buffer containing first DTT (100 mg/10 mL) and then iodoacetamide (250 mg/10 mL) for 35 min each. The second dimension was finally performed on a 10% polyacrylamide gel for 1.5 h at 110 V. In the end, the gel was stained overnight with a specific blue stain containing Coomassie Brilliant Blue G250 (BioRad) (0.1% Coomassie Brilliant Blue G250, 10% $NH_4 2SO_4$ and 2% H_3PO_4; the solution was mixed with 20% methanol before use).

Spots of interest were excised and processed using trypsin recombinant, Proteomics Grade kit (Roche, n code: 3,708,985,001), according to the manufacturer's protocol. Peptides were resuspended in 7 µL of 0.1% TFA.1 µL of each protein sample was quickly mixed with 1 µL of matrix (*α-cyano-4-hydroxycinnamic acid*) (Sigma Aldrich, n code: 476,870) and put on the appropriate plate for the identification at Microflex LRF Maldi-TOF mass spectrometer (Bruker Daltonics, Germany)[49]. Protein identification was carried out by searching the Mascot protein database. The parameters used for the search of a protein database with PMF (peptide mass fingerprinting) were as follows: enzyme, trypsin,species, *Dictyostelium discoideum*; pI range, ± 1; Mr range, ± 20%; missed cleavage sites allowed, 1; minimum peptide hits, 4; mass tolerance, ± 100 ppm; modifications, cysteine treated with iodoacetamide to carboxamidomethyl and methionine in the oxidized form.

Results

Impaired proliferation of *Dictyostelium* cells upon exposure to PCB 138 and PCB 153

The growth assay was performed by growing Ax4 cells with increasing concentrations (50 µM, 100 µM and 200 µM) of PCB 138 or PCB 153, and cell proliferation was monitored over 3 days. Results shown in Fig. 1 revealed a significant reduction in the number of cell generations compared to the untreated control (Vehicle). Notably, the inhibitory effect was already evident at 50 µM, the lowest tested concentration (50 µM) and became more pronounced at higher doses. While both congeners exerted a comparable growth- inhibitory effect, PCB 138 showed a statistically stronger reduction at 100 µM compared to PCB 153. In fact, the number of generations reached on the 3rd day was lower in treated cells, indicating that treated cells completed fewer generations than the control by day 3. Growth curves nevertheless progressed into the exponential phase and reached plateau without abrupt interruptions or marked drops in cell density, suggesting a slower net proliferation rate than

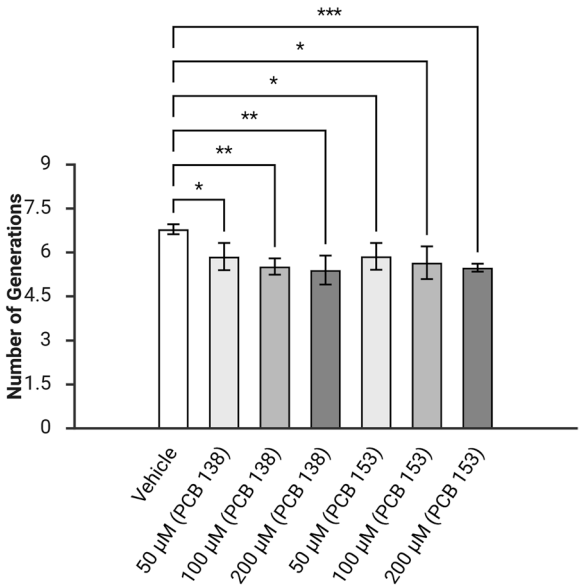

Fig. 1. *Dictyostelium* growth assay in presence of PCBs. Ax4 cells were grown in presence of PCB 138 or 153 at increasing concentrations (50 µM, 100 µM and 200 µM). The graph shows the number of generations reached on the 3rd day of growth. Data represent ± standard deviation of three independent biological replicates. Statistical significance was assessed using One-way ANOVA with Dunnett's multiple comparisons test (*$p < 0.05$, **$p < 0.01$, *** $p < 0.001$). This graph was generated with BioRender.

an arrest or massive cell death. Based on these findings, 50 µM was selected as the working concentration for subsequent functional assays.

PCBs induce the formation of small-fruiting-body phenotype

After assessing the effects of PCBs on cellular proliferation, we next examined their impact on *Dictyostelium* development, selecting a concentration of 50 µM due to its clear biological effect while avoiding acute cytotoxicity. Basically, cells were cultured in absence of nutrients, on phosphate agar (agar P), to prime the development process with either PCB 138 or PCB 153 added directly to the agar in separate experiments as shown in Fig. 2, PCBs exposure altered the normal aggregation pattern. After 5 h (T5) of starvation, treated cells showed shorter and less organized streams compared to vehicle controls. Mound formation was also delayed and reduced in size at 8 h (T8). By 24 and 48 h (T24—T48), a marked small-fruiting-body phenotype was observed in treated samples, with some aggregates failing to culminate even after 48 h. Cells were intentionally monitored for up to 48 h to evaluate whether delayed development could compensate for the observed defects. Similar results were obtained when cells were pretreated in suspension for 3 days before plating (Fig. S1), confirming the robustness of the phenotype.

PCBs reduce THP-1 cells viability and downregulate *hamp* gene expression

According to PCBs inhibitory effect on *Dictyostelium* growth, and to explore whether similar toxic effects of both PCBs selected for the project could be observed in cell lines, a vitality assay (XTT assay) was performed on THP-1 cells, a line of monocytes isolated from peripheral blood from an acute monocytic leukemia patient. Cells were treated for 3 days with increasing concentrations (1 µM, 10 µM, 50 µM and 100 µM) of each PCB. As shown in Fig. 3A, PCB 153 significantly reduced cell viability starting from 10 µM, while PCB 138 caused a significant reduction only at 50 µM. The highest tested concentrations of both PCBs (100 µM) further exacerbated the effect. Given the known impact of PCBs on iron metabolism, we measured the expression *hamp* gene encoding Hepcidin, a key regulator of iron homeostasis. As shown in Fig. 3B, *hamp* was significantly downregulated following exposure to PCB 138, supporting the relevance of the iron-regulatory pathway in the cellular response to PCBs toxicity.

Developmental and iron-dependent genes expression are affected by PCBs action

Based on our findings on PCBs-induced alterations in *Dictyostelium* growth and development, and considering the established link between PCBs and iron homeostasis in human, we assessed the expression of iron regulatory and cAMP genes expression by qPCR. As shown in Fig. 4A, Ax4 *Dictyostelium* cells treated with PCB 138 produced a different expression pattern of iron-dependent genes. Specifically, cells treated with PCB 138 exhibited a significant upregulation in the expression of *ABC transporter B7* (*abcB7*) and *ferroportin* (*fpn*) genes with fold increases of 4.6 and 1.6, respectively, while *ferritin* (*ferr*) gene was markedly downregulated, indicating a disruption in iron storage and efflux mechanisms. In contrast, PCB 153 did not induce significant changes in these genes. Other iron-related genes, including *aconitase 1* (*aco1*), *frataxin* (*fxn*) and *mitoferrin* (*mcfF*) remained largely unaffected by either congener.

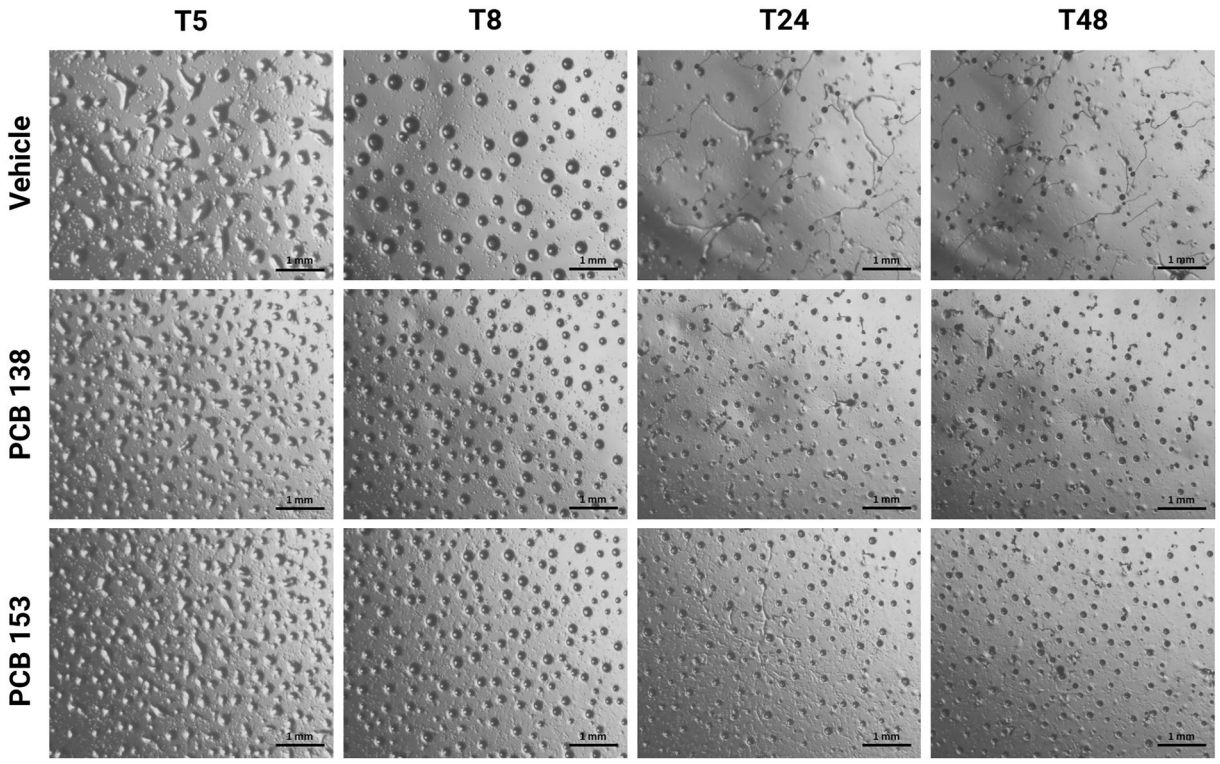

Fig. 2. *Dictyostelium* development assay in presence of PCBs. Ax4 cells were starved on agar P to initiate the development process. PCB 138 and 153 were added directly into the agar at a concentration of 50 µM. The figure shows representative images at different time points: T5 (5 h), T8 (8 h), T24 (24 h), and T48 (48 h). Images were captured using a digital microscope imager (Celestron) at 10X magnification (scale bar = 1 mm). The panel shown the correspond to the original images obtained.

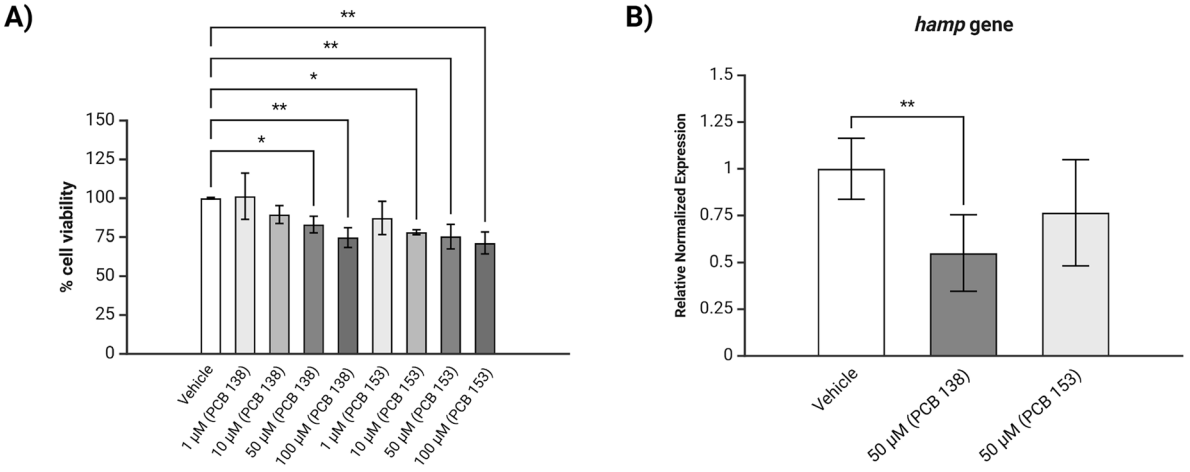

Fig. 3. Effects of PCB 138 and PCB 153 on THP-1 cells viability and *hamp* gene expression. **A**) Cell vitality was assessed using the MTT assay. PCBs were used at different concentrations (1 µM, 10 µM, 50 µM and 100 µM). The experiment was seeded in triplicate. **B**)*hamp* gene expression was analyzed by qPCR after treatment with 50 µM of each PCB. Three independent replicates were used for relative expression data analysis. Statistical significance was performed using One-way ANOVA with Dunnett's multiple comparisons test for both experiments (* = $p < 0.05$, ** = $p < 0.01$, *** = $p < 0.001$). This figure was generated with BioRender.

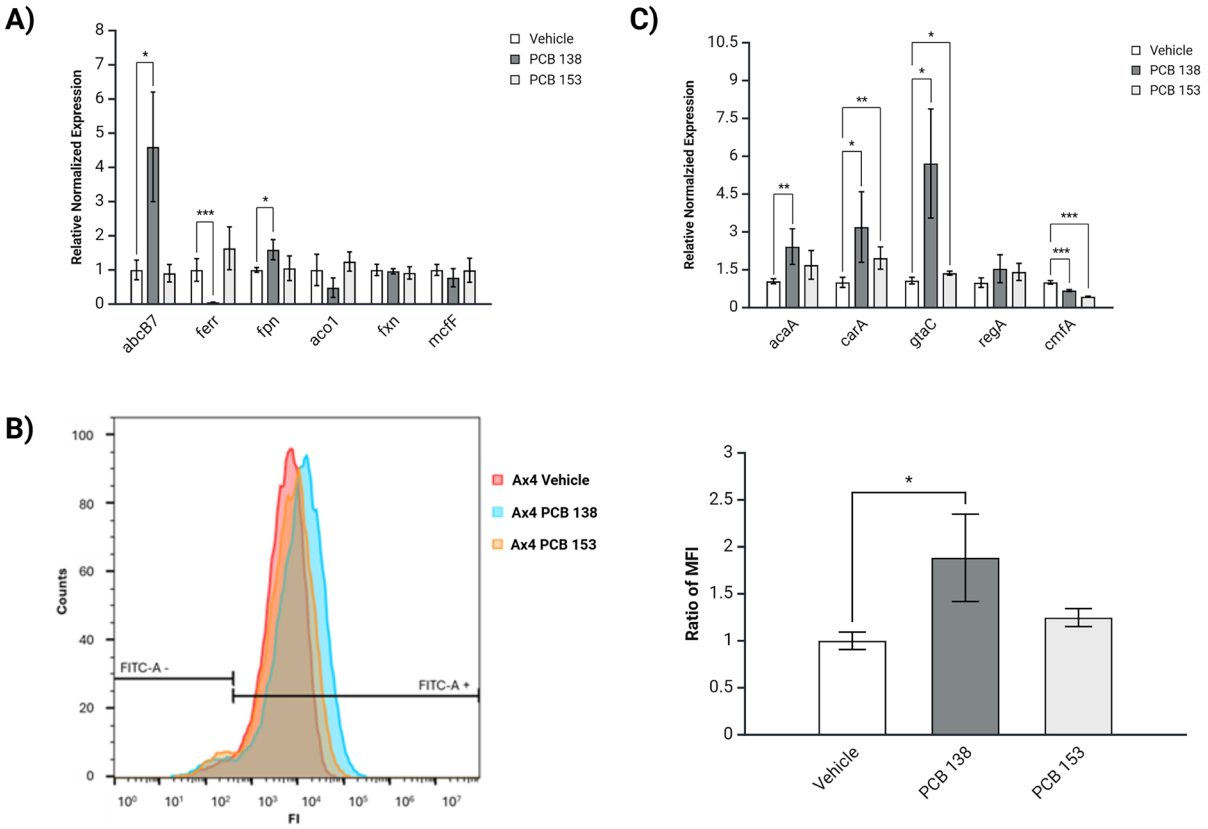

Fig. 4. Expression of iron-related and cAMP signaling pathways genes following PCB treatments and assessment of intracellular iron levels following PCB exposure. Ax4 cells were treated for 3 days with PCB 138 and PCB 153 (50 μM) before the analysis. The relative expression of iron-related **(A)** and developmental **(C)** genes are reported in the graphs. Intracellular iron level was indirectly measured through calcein fluorescence quenching assay **(B)**. Flow cytometry profiles (left panel) and mean fluorescence intensity (MFI) ratio quantification (right panel) are shown. Vehicle sample was set as control (= 1). Data are presented as mean values from three independent biological replicates. Statistical significance was determined for both experiments using One-way ANOVA with Dunnett's multiple comparisons test (* = $p < 0.05$, ** = $p < 0.01$, *** = $p < 0.001$). This graph was generated with BioRender.

To corroborate these findings, intracellular iron levels were indirectly measured using calcein fluorescence quenching assay. As depicted in Fig. 4B, flow cytometry quenching analysis revealed that the mean fluorescence intensity (MFI) of calcein was higher in cells treated with PCB 138 compared to vehicle sample, suggesting a reduction in intracellular iron level in PCB138-treated cells. This reduction was less evident PCB 153 cells treated.

We next analyzed genes involved in aggregation and differentiation, key processes regulated by cAMP signaling in *Dictyostelium*. the effects of both PCBs were more consistent compared with those of the iron related genes. After a 5-h starvation of Ax4 cells, PCB 138 significantly upregulated the expression of several key genes involved in cAMP signaling pathway. These genes included *adenylate cyclase A* (*acaA*), *cyclic AMP receptor A* (*carA*), *GATA transcription factor* (*gtaC*) genes, as reported in Fig. 4C. Notably, although *regA* mRNA levels did not show a statistically significant change upon PCB treatment, a clear upregulation of RegA protein was detected by western blot analysis (Fig. S2). PCB 153 treatment had less pronounced effect on the expression of these developmental genes compared to PCB 138. In addition, we evaluated the expression of *conditioned medium factor A* (*cmfA*) expression, a gene involved in sensing cell density and coordinating the early stages of aggregation. A significant downregulation of *cmfA* was detected in PCB-treated cells, suggesting that PCBs may interfere with cell–cell communication signals essential for proper morphogenesis. This impairment could contribute to the formation of smaller aggregates observed in treated samples. The full list of analyzed genes is reported in Table 1.

PCBs induce oxidative stress and alter mitochondrial morphology in *Dictyostelium*

To investigate whether PCB exposure leads to oxidative stress in *Dictyostelium*, intracellular reactive oxygen species (ROS) level was measured using the DHE-based fluorescence assay. As shown in Fig. 5A, cells treated with PCB 138 or PCB 153 exhibited an increased fluorescence signal compared to vehicle ones. This trend was confirmed by calculating the ROS production rate over time (RFU/min), which revealed to be significant upon

Gene product	Localization	Gene name	Dictybase ID
Adenylate cyclase A	plasma membrane	*acaA*	DDB_G0281545
cAMP receptor A	plasma membrane	*carA*	DDB_G0273397
GATA transcription factor	cytosol, nucleus	*gtaC*	DDB_G0277589
cAMP phosphodiesterase	cytosol	*regA*	DDB_G0284331
ABCB7	mitochondrial membrane	*abcB7*	DDB_G0269720
Aconitase 1	cytosol	*aco1*	DDB_G0279159
Frataxin	mitochondrion	*fxn*	DDB_G0293246
Mitoferrin	mitochondrial membrane	*mcfF*	DDB_G0269470
Slc 40 family protein	plasma membrane	*fpn*	DDB_G0279065
Ferritin-like superfamily protein	cytosol	*ferr*	DDB_G0278989
Conditioned medium factor A	extracellular space	*cmfA*	DDB_G0275007
Superoxide dismutase 1	cytosol, mitochondrion	*sod1*	DDB_G0290343
Superoxide dismutase 2	mitochondrion	*sod2*	DDB_G0271106
Superoxide dismutase A	phagocytic vesicle	*sodA*	DDB_G0267420
Superoxide dismutase B	plasma membrane	*sodB*	DDB_G0283021

Table 1. List of analysed *Dictyostelium* genes with corresponding gene product, localization, gene name and Dictybase ID.

treatment with both PCBs. Moreover, according to the ratio of RFU/min, PCB 153 turned out to have a stronger effect compared to its congener, as reported in Fig. 5B.

To support these findings, we evaluated the expression genes encoding superoxide dismutases, shown in Fig. 5C. Notably, both PCB 138 and PCB 153 significantly downregulated *superoxide dismutase 1* (*sod1*) gene. Additionally, PCB 138 treatment caused a marked decrease in *superoxide dismutase 2* (*sod2*) and *B* (*sodB*) transcript levels. In contrast, *superoxide dismutase A* (*sodA*) expression remained largely unchanged following exposure to either congener. These results suggest that PCBs impair the antioxidant defense system, potentially amplifying oxidative stress. A complete list of analyzed genes is provided in Table 1.

To assess the impact of oxidative stress on mitochondria structure, we performed a confocal microscopy analysis of Ax4 cells expressing the mitochondrial marker Fxn-GFP (Ax4::Fxn-GFP). As depicted in Fig. 5D, mitochondrial morphology was profoundly affected by both PCBs, with mitochondria appearing fragmented and less interconnected compared to control cells. As shown in Fig. 5E, image analysis through ImageJ MiNa tool revealed a significant reduction in both mitochondrial branches length and network branches mean (index of branches interconnection) in PCB-treated cells. However, the overall mitochondrial area (footprint) was not significantly altered. Together, these results confirm that PCB 138 and PCB 153 promote oxidative stress in *Dictyostelium* associated with transcriptional repression of antioxidant genes and structural mitochondria alteration. This graph was generated with BioRender.

PCB 138 alter the proteomic profile in *Dictyostelium*

To gain deeper insights into the molecular pathways affected by PCB exposure, we performed two-dimensional electrophoresis (2D-E) on protein extracts from Ax4 cells treated with PCB 138. Comparative analysis of proteomic profiles between treated and vehicle cells revealed noticeable differences, as shown in Fig. 6. Among the 55 gel spots that were collected, 31 were fully characterized (Table S2) including 11 that were differentially expressed between the conditions. Identified differentially expressed proteins are shown in Table 2. A classification, based on Gene Ontology (GO) terms associated to each protein revealed functional enrichment in several biological processes. Specifically, four (CAD1, CAP, CGL and EF1A1) were associated with the development process including aggregation and sporocarp formation, while two HS7C2 and MDH2 were linked to stress response. Four additional proteins (ARGE, CGL, METK and MSDH) were involved in amino acid biosynthesis or catabolism, and one (PAP1A) was implicated in mRNA processing.

Notably, the development protein CAD1 exhibited a distinct shift in isoelectric point (pI) upon treatment. In vehicle cells, CAD1 was detected as spot 1, whereas in PCB-treated samples, a second form (spot 9) with a different pI was also identified as CAD1, suggesting possible post-translational modification or alternative isoform expression induced by PCB exposure.

Discussion

To gain insight into the cellular mechanisms underlying PCB toxicity, we used *Dictyostelium discoideum* as our primary model system, leveraging its unique ability to link unicellular proliferation and multicellular development with conserved regulatory pathways. This allowed us to explore the molecular, physiological, and developmental consequences of exposure to two widespread PCBs (138 and 153), uncovering conserved and compound-specific effects across species.

Our results demonstrate that both PCB 138 and PCB 153 impair *Dictyostelium* cell cycle, by interfering with processes essential for sustained proliferation and development. Exposure to PCB 138 and 153 results in a measurable slowdown in *Dictyostelium* Ax4 growth, as evidenced by a reduced number of generations completed within the experimental time. However, growth curves reached the stationary phase without abrupt

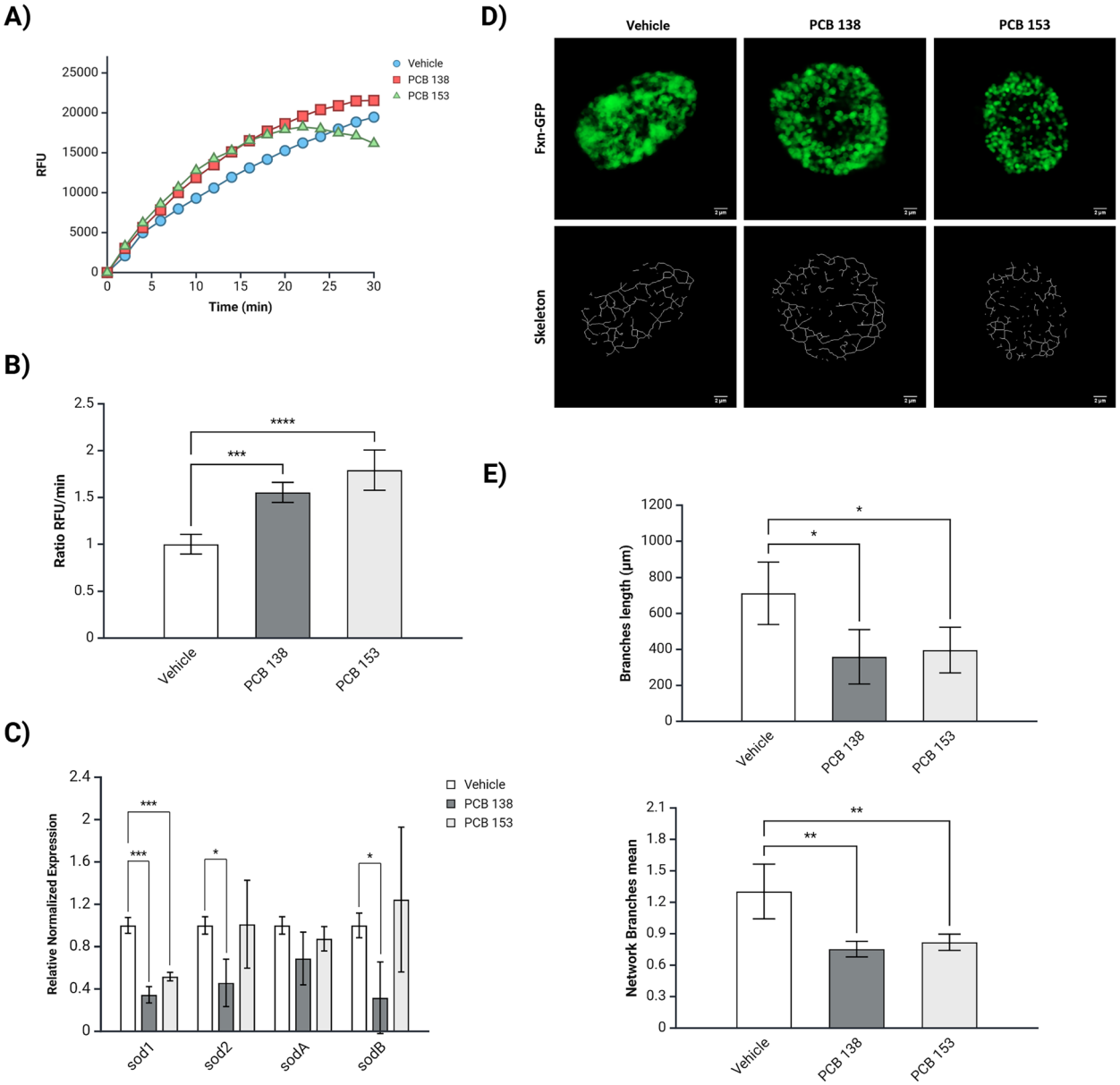

Fig. 5. Assessment of ROS accumulation, antioxidant gene expression, and mitochondrial network alterations after PCBs treatment in *Dictyostelium*. Ax4 cells were treated with 50 µM of PCB 138 or PCB 153 for 3 days. **(A)** ROS levels were indirectly measured by adding DHE to the cells and monitoring fluorescence over time (emission/excitation 560/590 nm, ± 20 nm). **(B)** Quantification of ROS production rates expressed as relative fluorescence units (RFU). Vehicle sample was used as control (= 1). **(C)** Expression levels of genes involved in oxidative stress response (*sod1*, *sod2*, *sodA* and *sodB*) were evaluated by qPCR. **(D)** Confocal imaging of mitochondrial morphology was performed on Ax4 cells expressing Fxn-GFP, and images were skeletonized for morphometric analysis (63x/1.40 oil objective; scale bar = 2 µm). The panel shown correspond to the original confocal images obtained. **(E)** ImageJ MiNa plugin was used to measure the ratio of mitochondrial area (footprint), branches length (µm) and network branches mean (mean number of connected lines for each structure). Three independent biological replicates were used for ROS measurement and qPCR data analysis. One-way ANOVA with Dunnett's multiple comparisons test was used for statistical significance (* = $p < 0.05$, ** = $p < 0.01$, *** = $p < 0.001$, **** = $p < 0.0001$).

interruptions or marked drops in cell density. This behavior is more consistent with a slower proliferation rate rather than acute cytotoxicity, supporting the view that these congeners function most likely through impairment of cellular processes such as iron homeostasis rather than by triggering extensive cell death. The differing concentration ranges of PCBs applied to *Dictyostelium* versus THP-1 cells are grounded in prior observations and reflect the distinct biological sensitivities of each model system. In fact, lower concentrations of PCBs (1 and 10 µM) were tested, but did not affect *Dictyostelium* growth, due to its well-known resistance

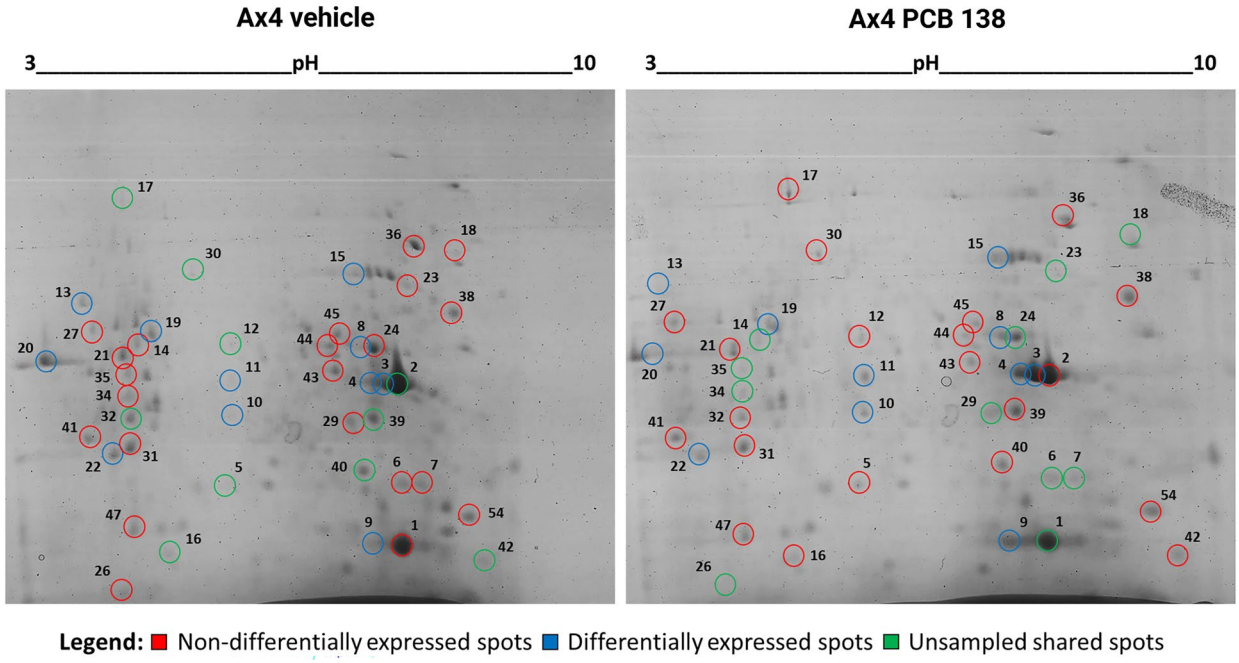

Fig. 6. Comparative 2D-electrophoresis analysis of *Dictyostelium* proteome following PCB 138 treatment. Representative 2D gels from untreated (Ax4 vehicle) and PCB 138 treated *Dictyostelium* cells are shown. Proteins were separated by isoelectric focusing (pH 3–10 NL) and SDS-PAGE, then stained with brilliant blue Coomassie. Proteins of collected gel spots were identified through Maldi-TOF analysis. Red circles represent non-differentially expressed proteins, while blue circles correspond to differentially expressed ones. Green circles are, instead, unsampled protein spots that are in common between the two gels. Uncropped gel images can be found in raw data file.

Spot number	Differentially expressed identified proteins	Relative expression	GO
8	**ARGE** (Acetylornithine deacetylase)	Upregulated	arginine/ornithine biosynthesis
9	**CAD1** (Calcium-dependent cell adhesion molecule 1)	Upregulated	sorocarp development, cell–cell adhesion
10	**CGL** (Cystathionine gamma-lyase)	Upregulated	cysteine/L-methionine biosynthesis
11	**METK** (S-adenosylmethionine synthase)	Upregulated	S-adenosylmethionine synthesis
13	**PAP1A** (Polyadenylate-binding protein 1-A)	Downregulated	mRNA processing
15	**HS7C2** (Heat schok cognate 70 kDa protein 2)	Upregulated	stress response
19	**CAP** (Adenylyl cyclase-associated protein)	Upregulated	aggregation, sorocarp development
20	**EF1A1** (Elongation factor 1-alpha)	Downregulated	actin filament bundle assembly
22	**MDH2** (probable Malate dehydrogenase 2, mitochondrial)	Upregulated	oxidation–reduction process, TCA cycle
22	**MSDH** (probable Methylmalonate-semialdehyde dehydrogenase, mitochondrial)	Upregulated	oxidation–reduction process, valine degradation

Table 2. List of 2D-electrophoresis differentially expressed proteins identified through Maldi-TOF analysis.

to environmental contaminants[50,51]. In contrast, mammalian cells, such as THP-1 cell line, are generally more susceptible. Consequently, lower PCBs concentrations were used for THP-1 cells, according to other similar studies found in literature[52–54].

These functional phenotypes were underpinned by major alterations in intracellular iron homeostasis, cAMP signaling, oxidative stress levels, and mitochondrial integrity. Importantly, by integrating gene expression profiling, flow cytometry, fluorescence microscopy and proteomics, we provide a comprehensive map of the cellular impact of PCB exposure.

During the growth phase, we observed that the exposure to both PCB 138 and PCB 153 reduced the proliferation rate. Given the known role of iron in supporting cell proliferation and metabolism, we hypothesized that PCBs may affect iron availability. This was confirmed in THP-1 cells, where PCB 138, but not PCB 153, downregulated the *hepcidin* (*hamp*) gene, a master regulator of systemic iron level. Consequently, we can infer that lower hepcidin levels upon PCB 138 exposure facilitate increased iron efflux from cells into the extracellular matrix. This reduction in intracellular iron levels can disrupt the delicate balance of iron homeostasis and increase oxidative stress, both of which are crucial for maintaining cellular health[13,14,19,20,55].

This observation prompted us to explore whether a similar iron-dependent mechanism might operate in *Dictyostelium*. PCB 138 exposure led to altered expression of several iron-related genes: *abcB7* and *fpn* were upregulated, while *ferr* and *aco1* were downregulated. Flow cytometry with calcein quenching further confirmed a reduction in intracellular iron, supporting the idea of increased efflux. These changes suggest a model in which PCB 138 triggers mitochondrial iron release via *abcb7* upregulation, coupled with ferroportin-mediated export, ultimately depleting cytosolic iron and impairing iron-requiring processes, including proliferation and mitochondrial function. For instance, non-dioxin-like congeners such as PCB 77 and PCB 153 have been shown to suppress hepcidin expression, thereby disturbing the hepcidin–ferroportin regulatory axis and altering systemic iron metabolism[56]. Epidemiological studies further support this connection, reporting positive associations between serum PCB burden and circulating iron levels in humans[18]. These findings suggest that monitoring PCB exposure could be relevant in diseases where iron dysregulation contributes to pathogenesis, highlighting a potential mechanistic link between environmental contaminants and systemic iron homeostasis. It is important to note that calcein assay does not necessarily reflect changes exclusively in intracellular iron, since its fluorescent signal can be quenched by other metals. Nonetheless, the convergence of our data strongly indicates that alterations in intracellular iron homeostasis are driven by PCB exposure.

Concomitantly, we observed a marked oxidative stress response. ROS level was significantly increased, and several *sod* genes were downregulated, which typically occurs under persistent oxidative pressure. Multiple studies have demonstrated that PCBs and their metabolites induce[57–59]. Importantly, PCB-derived semiquinones and quinones can undergo redox cycling, exacerbating ROS production and compromising antioxidant defenses[60,61]. Moreover, genotoxic effects consistent with oxidative DNA damage have been observed in studies where PCB exposure was associated with lipid peroxidation, caspase activation and DNA adduct formation[14,62,63]. All this evidence supports the role of PCBs as contributing factors in tumor development and highlights the crucial need to continue studying the effects of environmental pollutants. Mitochondrial morphology was visibly altered, shifting toward fragmented and less branched networks. These data reinforce the hypothesis that iron depletion and ROS production are intertwined consequences of PCBs toxicity. Despite structural similarity, PCB 153 induced much weaker molecular and phenotypic effects. This highlights the importance of subtle differences in PCB congener chemistry (such as bond position and rotational flexibility) which may dictate their interaction with cellular targets. Similar proliferation inhibiting effects of non-dioxin like PCBs have been reported in mammalian cell lines, often linked to mitochondrial dysfunction and altered metabolism[6]. Our finding extended these observations to a simple model as *Dictyostelium*, reinforcing the evolutionary conservation of these pathways. This is consistent with previous reports of hepcidin suppression by PCBs[18,19] and could represent a unifying mechanism across species. The decreased expression in *ferroportin* gene in *Dictyostelium* suggests that PCB exposure may affect an ancestral iron-regulatory pathway functionally analogous to the vertebrate hepcidin-ferroportin axis. While *Dictyostelium* lacks hepcidin, the observed molecular changes point to conserved principles in iron efflux regulation that could be relevant to both environmental toxicology and human hematological health.

Beyond growth inhibition, PCBs had strong impact on development. Even at sub-cytotoxic doses, exposed cells formed smaller aggregates and fruiting bodies, correlating with downregulation of *cmfA*, a gene critical for sensing cell density and initiating proper aggregation. Aggregation in *Dictyostelium* relies on cAMP signaling and cell–cell adhesion via Counting factor (CFF) and Conditioned Medium Factor (CMF)[64]. We also found several key regulators of aggregation and differentiation in the cAMP signaling pathways (*acaA*, *carA*, *gtaC* and regA) were upregulated by PCB 138, suggesting disrupted signaling feedback loops.

Of note, gtaC, orthologous to human GATA-3 and a known downstream target of the hepcidin pathway, was significantly induced. In mammalian systems, GATA-3 has been implicated in modulation of iron status through hepcidin-ferroportin signaling[21]. The upregulation of *gtatC* gene in *Dictyostelium*, an organism that lacks a direct hepcidin ortholog, suggest that an ancestral iron responsive transcriptional circuit may link PCB-induced iron depletion to development reprogramming, pointing to a conserved regulatory axis shared with human cells.

Proteomic analysis further corroborated the transcriptomic findings, identifying proteins involved in stress responses (HS7C2, MDH2), development (CAD1, CAP, EF1A1), and amino acid metabolism (CGL, METK, MSDH). The shift in isoelectric point of CAD1 in treated samples suggests possible post-translational modification, such as phosphorylation or glycosylation, that could alter the protein's charge and conformation[65].

Since CAD1 is a calcium-dependent cell adhesion protein, such changes may impair its ability to mediate stable cell–cell contacts during the first hours of development. This defect, in combination with the PCB-induced dowregulation of *cmfA* expression is likely to weaken both adhesion and intracellular communication. We suggest that together these alterations could contribute to the formation of the smaller and less organized aggregates observed in cells exposed to PCB.

Conclusion

This study highlights *Dictyostelium* as a powerful model organism for investigating the cellular effects of environmental pollutants. We demonstrate that exposure to PCB 138- and to a lesser extent PCB 153- disrupt the finely tuned process of growth and development suggesting a delicate balance between signaling molecules, environmental factors, and cell behavior, altering the cellular redox state or through other stress-related pathways.

Our findings suggest that *Dictyostelium* harbors an evolutionarily conserved core response to PCB toxicity, mechanistically linked to iron metabolism and ROS regulation. This poses *Dictyostelium*.

not only as a sensitive biosensor but also as a mechanistic model to study conserved toxicological pathways. Moreover, the versatility and genetic tractability of *Dictyostelium* make it a suitable candidate for use in environmental biomonitoring. Its presence, behavior and genomic adaptations in polluted versus pristine soil could serve as robust indicators of soil quality. Future directions may involve genome-wide association studies on *Dictyostelium* clones from different environments, uncovering pollutant-specific adaptation signatures.

In summary, our study provides new evidence for how structurally related PCBs elicit distinct biological responses and underscores the relevance of *Dictyostelium* as a cross-species model to explore the fundamental principles of environmental toxicity.

Data availability

All data generated or analyzed during this study are included in this published article and its supplementary information files. We have uploaded the raw data in Related files section to ensure access for the Editor and reviewers during peer review, and are available from the corresponding author upon request.

Received: 30 June 2025; Accepted: 23 September 2025
Published online: 29 October 2025

References

1. Guo, W. et al. Persistent Organic Pollutants in Food: Contamination Sources, Health Effects and Detection Methods. *Int. J. Environ. Res. Public Health* **16**(22), 4361. https://doi.org/10.3390/ijerph16224361 (2019).
2. Schettgen, T., Alt, A., Preim, D., Keller, D. & Kraus, T. Biological monitoring of indoor-exposure to dioxin-like and non-dioxin-like polychlorinated biphenyls (PCB) in a public building. *Toxicol. Lett.* **213**(1), 116–121. https://doi.org/10.1016/j.toxlet.2011.06.005 (2012).
3. Antignac, J. P. et al. Country-specific chemical signatures of persistent organic pollutants (POPs) in breast milk of French Danish and Finnish women. *Environ. Pollut.* **218**, 728–738. https://doi.org/10.1016/j.envpol.2016.07.069 (2016).
4. Anttila, P., Brorström-Lundén, E., Hansson, K., Hakola, H. & Vestenius, M. Assessment of the spatial and temporal distribution of persistent organic pollutants (POPs) in the Nordic atmosphere. *Atmos. Environ.* **140**, 22–33. https://doi.org/10.1016/j.atmosenv.2016.05.044 (2016).
5. Lopez-Garcia, M. et al. Endocrine Disruptors and Attention Deficit Hyperactivity Disorder: A Systematic Review. *Arch. Med. Res.* **56**(7), 103260. https://doi.org/10.1016/j.arcmed.2025.103260 (2025).
6. Knerr, S. & Schrenk, D. Carcinogenicity of "non-dioxinlike" polychlorinated biphenyls. *Crit. Rev. Toxicol.* **36**(9), 663–694. https://doi.org/10.1080/10408440600845304 (2006).
7. IARC monographs on the evaluation of the carcinogenic risk of chemicals to humans. Polychlorinated biphenyls and polybrominated biphenyls. *IARC Monogr. Eval. Carcinog. Risk. Chem. Hum.* **18**, 1–124 (1978).
8. Cao, J., Fan, T., Li, W. & Xiao, S. Association study between plasma levels of polychlorinated biphenyls and risk of cutaneous malignant melanoma. *Environ. Int.* **126**, 298–301. https://doi.org/10.1016/j.envint.2019.02.014 (2019).
9. Faroon, O. & Ruiz, P. Polychlorinated biphenyls: New evidence from the last decade. *Toxicol. Ind. Health* **32**(11), 1825–1847. https://doi.org/10.1177/0748233715587849 (2016).
10. Burns, J. S. et al. Associations of peri-pubertal serum dioxins and polychlorinated biphenyls with growth and body composition among Russian boys in a longitudinal cohort. *Int. J. Hyg. Environ. Health* **223**(1), 228–237. https://doi.org/10.1016/j.ijheh.2019.08.008 (2020).
11. Freeman, M. D. & Kohles, S. S. Plasma levels of polychlorinated biphenyls, non-Hodgkin lymphoma, and causation. *J. Environ. Public Health* **2012**, 258981. https://doi.org/10.1155/2012/258981 (2012).
12. Santoro, A. et al. Polychlorinated Biphenyls (PCB 101, 153, and 180) Impair Murine Macrophage Responsiveness to Lipopolysaccharide: Involvement of NF-κB Pathway. *Toxicol. Sci.* **147**(1), 255–269. https://doi.org/10.1093/toxsci/kfv127 (2015).
13. Ward, M. H. et al. Residential exposure to polychlorinated biphenyls and organochlorine pesticides and risk of childhood leukemia. *Environ. Health Perspect.* **117**(6), 1007–1013. https://doi.org/10.1289/ehp.0900583 (2009).
14. Liu, J., Tan, Y., Song, E. & Song, Y. A Critical Review of Polychlorinated Biphenyls Metabolism, Metabolites, and Their Correlation with Oxidative Stress. *Chem. Res. Toxicol.* **33**(8), 2022–2042. https://doi.org/10.1021/acs.chemrestox.0c00078 (2020).
15. Dreiem, A., Rykken, S., Lehmler, H. J., Robertson, L. W. & Fonnum, F. Hydroxylated polychlorinated biphenyls increase reactive oxygen species formation and induce cell death in cultured cerebellar granule cells. *Toxicol. Appl. Pharmacol.* **240**(2), 306–313. https://doi.org/10.1016/j.taap.2009.07.016 (2009).
16. Lai, I. et al. Acute toxicity of 3,3',4,4',5-pentachlorobiphenyl (PCB 126) in male Sprague-Dawley rats: effects on hepatic oxidative stress, glutathione and metals status. *Environ. Int.* **36**(8), 918–923. https://doi.org/10.1016/j.envint.2009.11.002 (2010).
17. Coteur, G. et al. Effects of PCBs on reactive oxygen species (ROS) production by the immune cells of Paracentrotus lividus (Echinodermata). *Mar. Pollut. Bull.* **42**(8), 667–672. https://doi.org/10.1016/s0025-326x(01)00063-7 (2001).
18. Henríquez-Hernández, L. A. et al. Relationship of polychlorinated biphenyls (PCBs) with parasitism, iron homeostasis, and other health outcomes: Results from a cross-sectional study on recently arrived African immigrants. *Environ. Res.* **150**, 549–556. https://doi.org/10.1016/j.envres.2015.07.017 (2016).
19. Qian, Y. et al. Polychlorinated biphenyls (PCBs) inhibit hepcidin expression through an estrogen-like effect associated with disordered systemic iron homeostasis. *Chem. Res. Toxicol.* **28**(4), 629–640. https://doi.org/10.1021/tx500428r (2015).
20. Nemeth, E. & Ganz, T. Hepcidin and Iron in Health and Disease. *Annu. Rev. Med.* **74**, 261–277. https://doi.org/10.1146/annurev-med-043021-032816 (2023).
21. Camaschella, C., Nai, A. & Silvestri, L. Iron metabolism and iron disorders revisited in the hepcidin era. *Haematologica* **105**(2), 260–272. https://doi.org/10.3324/haematol.2019.232124 (2020).
22. Nemeth, E. & Ganz, T. Hepcidin-Ferroportin Interaction Controls Systemic Iron Homeostasis. *Int. J. Mol. Sci.* **22**(12), 6493. https://doi.org/10.3390/ijms22126493 (2021).
23. Ni, S., Yuan, Y., Kuang, Y. & Li, X. Iron Metabolism and Immune Regulation. *Front. Immunol.* **13**, 816282. https://doi.org/10.3389/fimmu.2022.816282 (2022).
24. Mehdiabadi, N. J. et al. Social evolution: kin preference in a social microbe. *Nature* **442**(7105), 881–882. https://doi.org/10.1038/442881a (2006).
25. Bloomfield, G. et al. Neurofibromin controls macropinocytosis and phagocytosis in Dictyostelium. *Elife* **4**, e04940. https://doi.org/10.7554/eLife.04940 (2015).
26. Pears, C. J. & Gross, J. D. Microbe Profile: Dictyostelium discoideum: model system for development, chemotaxis and biomedical research. *Microbiol. (Reading)* https://doi.org/10.1099/mic.0.001040 (2021).
27. Bozzaro, S. The past, present and future of Dictyostelium as a model system. *Int. J. Dev. Biol.* **63**(8-9–10), 321–331. https://doi.org/10.1387/ijdb.190128sb (2019).
28. Biondo, M. et al. The Dynamics of Aerotaxis in a Simple Eukaryotic Model. *Front. Cell Dev. Biol.* **9**, 720623. https://doi.org/10.3389/fcell.2021.720623 (2021).
29. Thewes, S., Soldati, T. & Eichinger, L. Editorial: Amoebae as Host Models to Study the Interaction With Pathogens. *Front. Cell. Infect. Microbiol.* **9**, 47. https://doi.org/10.3389/fcimb.2019.00047 (2019).
30. Annesley, S. J. et al. Dictyostelium, a microbial model for brain disease. *Biochim. Biophys. Acta.* **1840**(4), 1413–1432. https://doi.org/10.1016/j.bbagen.2013.10.019 (2014).

31. Frej, A. D., Otto, G. P. & Williams, R. S. B. Tipping the scales: Lessons from simple model systems on inositol imbalance in neurological disorders. *Eur. J. Cell. Biol.* **96**(2), 154–163. https://doi.org/10.1016/j.ejcb.2017.01.007 (2017).
32. Alvarez-Curto, E. et al. cAMP production by adenylyl cyclase G induces prespore differentiation in Dictyostelium slugs. *Development* **134**(5), 959–966. https://doi.org/10.1242/dev.02775 (2007).
33. Dormann, D., Vasiev, B. & Weijer, C. J. The control of chemotactic cell movement during Dictyostelium morphogenesis. *Philos. Trans. R Soc. Lond. B Biol. Sci.* **355**(1399), 983–991. https://doi.org/10.1098/rstb.2000.0634 (2000).
34. Artemenko, Y., Lampert, T. J. & Devreotes, P. N. Moving towards a paradigm: common mechanisms of chemotactic signaling in Dictyostelium and mammalian leukocytes. *Cell. Mol. Life Sci.* **71**(19), 3711–3747. https://doi.org/10.1007/s00018-014-1638-8 (2014).
35. Meima, M. & Schaap, P. Dictyostelium development-socializing through cAMP. *Semin. Cell. Dev. Biol.* **10**(6), 567–576. https://doi.org/10.1006/scdb.1999.0340 (1999).
36. Schaf, J., Damstra-Oddy, J. & Williams, R. S. B. Dictyostelium discoideum as a pharmacological model system to study the mechanisms of medicinal drugs and natural products. *Int. J. Dev. Biol.* **63**(8-9–10), 541–550. https://doi.org/10.1387/ijdb.190228rw (2019).
37. Van Driessche, N. et al. Global transcriptional responses to cisplatin in Dictyostelium discoideum identify potential drug targets. *Proc. Natl. Acad. Sci. U. S. A.* **104**(39), 15406–15411. https://doi.org/10.1073/pnas.0705996104 (2007).
38. Balbo, A. & Bozzaro, S. A novel bioassay for evaluating soil bio-hazards using Dictyostelium as biosensor: validation and application to the BIO-BIO project. *Fresenius Environ. Bull.* **17**(8b), 1137–1143 (2008).
39. Dondero, F. et al. Cellular responses to environmental contaminants in amoebic cells of the slime mould Dictyostelium discoideum. *Comp. Biochem. Physiol. C Toxicol. Pharmacol.* **143**(2), 150–157. https://doi.org/10.1016/j.cbpc.2006.01.005 (2006).
40. Sforzini, S. et al. Relevance of the bioavailable fraction of DDT and its metabolites in freshwater sediment toxicity: New insight into the mode of action of these chemicals on Dictyostelium discoideum. *Ecotoxicol. Environ. Saf.* **132**, 240–249. https://doi.org/10.1016/j.ecoenv.2016.06.013 (2016).
41. Whitehead, T. P. et al. Concentrations of Persistent Organic Pollutants in California Children's Whole Blood and Residential Dust. *Environ. Sci. Technol.* **49**(15), 9331–9340. https://doi.org/10.1021/acs.est.5b02078 (2015).
42. Pergolizzi, B., Bozzaro, S. & Bracco, E. G-Protein Dependent Signal Transduction and Ubiquitination in Dictyostelium. *Int. J. Mol. Sci.* **18**(10), 2180. https://doi.org/10.3390/ijms18102180 (2017).
43. Pergolizzi, B., Bracco, E. & Bozzaro, S. A new HECT ubiquitin ligase regulating chemotaxis and development in Dictyostelium discoideum. *J. Cell. Sci.* **130**(3), 551–562. https://doi.org/10.1242/jcs.194225 (2017).
44. Ali, M. S. et al. The Downregulation of Both Giant HERCs, HERC1 and HERC2, Is an Unambiguous Feature of Chronic Myeloid Leukemia, and HERC1 Levels Are Associated with Leukemic Cell Differentiation. *J. Clin. Med.* **11**(2), 324. https://doi.org/10.3390/jcm11020324 (2022).
45. Fey, P., Kowal, A. S., Gaudet, P., Pilcher, K. E. & Chisholm, R. L. Protocols for growth and development of Dictyostelium discoideum. *Nat. Protoc.* **2**(6), 1307–1316. https://doi.org/10.1038/nprot.2007.178 (2007).
46. Gaudet, P., Fey, P. & Chisholm, R. Transformation of dictyostelium with plasmid DNA by electroporation. *CSH Protoc.* https://doi.org/10.1101/pdb.prot5103 (2008).
47. Valente, A. J., Maddalena, L. A., Robb, E. L., Moradi, F. & Stuart, J. A. A simple ImageJ macro tool for analyzing mitochondrial network morphology in mammalian cell culture. *Acta Histochem.* **119**(3), 315–326. https://doi.org/10.1016/j.acthis.2017.03.001 (2017).
48. Zhang, X. & Soldati, T. Detecting, visualizing and quantitating the generation of reactive oxygen species in an amoeba model system. *J. Vis. Exp.* **81**, e50717. https://doi.org/10.3791/50717 (2013).
49. Pergolizzi, B. et al. Subchronic nandrolone administration reduces cardiac oxidative markers during restraint stress by modulating protein expression patterns. *Mol. Cell. Biochem.* **434**(1–2), 51–60. https://doi.org/10.1007/s11010-017-3036-7 (2017).
50. Zhao, Y. et al. Exploring the mechanisms of cadmium tolerance and bioaccumulation in a soil amoeba. *Sci. Total Environ.* **965**, 178637. https://doi.org/10.1016/j.scitotenv.2025.178637 (2025).
51. Amaroli, A. The Effects of Temperature Variation on the Sensitivity to Pesticides: a Study on the Slime Mould Dictyostelium discoideum (Protozoa). *Microb. Ecol.* **70**(1), 244–254. https://doi.org/10.1007/s00248-014-0541-z (2015).
52. Ghosh, S. et al. Polychlorinated Biphenyls (PCB-153) and (PCB-77) absorption in human liver (HepG2) and kidney (HK2) cells in vitro: PCB levels and cell death. *Environ. Int.* **36**(8), 893–900. https://doi.org/10.1016/j.envint.2010.06.010 (2010).
53. Yazdi, F., Shoeibi, S., Yazdi, M. H. & Eidi, A. Effect of prevalent polychlorinated biphenyls (PCBs) food contaminant on the MCF7, LNCap and MDA-MB-231 cell lines viability and PON1 gene expression level: proposed model of binding. *Daru* **29**(1), 159–170. https://doi.org/10.1007/s40199-021-00394-9 (2021).
54. Senthilkumar, P. K. et al. Airborne polychlorinated biphenyls (PCBs) reduce telomerase activity and shorten telomere length in immortal human skin keratinocytes (HaCat). *Toxicol. Lett.* **204**(1), 64–70. https://doi.org/10.1016/j.toxlet.2011.04.012 (2011).
55. Liu, J. et al. Polychlorinated biphenyl quinone induces hepatocytes iron overload through up-regulating hepcidin expression. *Environ. Int.* **139**, 105701. https://doi.org/10.1016/j.envint.2020.105701 (2020).
56. Wang, L. et al. PCB-77 disturbs iron homeostasis through regulating hepcidin gene expression. *Gene* **532**(1), 146–151. https://doi.org/10.1016/j.gene.2013.09.023 (2013).
57. Oakley, G. G., Devanaboyina, U., Robertson, L. W. & Gupta, R. C. Oxidative DNA damage induced by activation of polychlorinated biphenyls (PCBs): implications for PCB-induced oxidative stress in breast cancer. *Chem. Res. Toxicol.* **9**(8), 1285–1292. https://doi.org/10.1021/tx960103o (1996).
58. Dong, H. et al. Polychlorinated biphenyl quinone-induced genotoxicity, oxidative DNA damage and γ-H2AX formation in HepG2 cells. *Chem. Biol. Interact.* **212**, 47–55. https://doi.org/10.1016/j.cbi.2014.01.016 (2014).
59. Spencer, W. A., Lehmler, H. J., Robertson, L. W. & Gupta, R. C. Oxidative DNA adducts after Cu(2+)-mediated activation of dihydroxy PCBs: role of reactive oxygen species. *Free Radic. Biol. Med.* **46**(10), 1346–1352. https://doi.org/10.1016/j.freeradbiomed.2009.02.005 (2009).
60. Song, Y. et al. Chlorination increases the persistence of semiquinone free radicals derived from polychlorinated biphenyl hydroquinones and quinones. *J. Org. Chem.* **73**(21), 8296–8304. https://doi.org/10.1021/jo801397g (2008).
61. Liu, J. et al. Polychlorinated biphenyl quinone metabolites lead to oxidative stress in HepG2 cells and the protective role of dihydrolipoic acid. *Toxicol. In Vitro.* **26**(6), 841–848. https://doi.org/10.1016/j.tiv.2012.04.028 (2012).
62. Mutlu, E. et al. Polychlorinated Biphenyls Induce Oxidative DNA Adducts in Female Sprague-Dawley Rats. *Chem. Res. Toxicol.* **29**(8), 1335–1344. https://doi.org/10.1021/acs.chemrestox.6b00146 (2016).
63. Schilderman, P. A. et al. Induction of DNA adducts by several polychlorinated biphenyls. *Environ. Mol. Mutagen.* **36**(2), 79–86. https://doi.org/10.1002/1098-2280(2000)36:2%3c79::aid-em1%3e3.0.co;2-e (2000).
64. Van Haastert, P. J., Bishop, J. D. & Gomer, R. H. The cell density factor CMF regulates the chemoattractant receptor cAR1 in Dictyostelium. *J. Cell. Biol.* **134**(6), 1543–1549. https://doi.org/10.1083/jcb.134.6.1543 (1996).
65. Karunaratne, C. V., Weldeghiorghis, T. K., West, C. M. & Taylor, C. M. Conformational changes associated with post-translational modifications of Pro(143) in Skp1 of Dictyostelium–a dipeptide model system. *J. Am. Chem. Soc.* **136**(43), 15170–15175. https://doi.org/10.1021/ja5033277 (2014).

Acknowledgements
We would like to express our sincere gratitude to Prof. Saglio and to the Drug Discovery and Clinic (DDC) for their continuous support, which made the realization of the PhD program possible.

Author contributions
Conceptualization: S.R., C.P, and B.P.; Methodology: S.R., C.P, V.S, A.F, G.B; Validation S.R, C.P, V.S, A.F, and G.B; Data Curation S.R, C.P and B.P; Writing—original draft: S.R, C.P and B.P; Writing—review and editing: S.R, C.P, and B.P.; Supervision: B.P. All authors have read and agreed to the published version of the manuscript. All authors have read and agreed to the published version of the manuscript.

Funding
This research was funded by University of Turin code: PERB_RIC_N_COMP_20_01 to B.P.

Declarations

Competing interests
The authors declare no competing interests.

Additional information
Supplementary Information The online version contains supplementary material available at https://doi.org/10.1038/s41598-025-21796-8.

Correspondence and requests for materials should be addressed to C.P. or B.P.

Reprints and permissions information is available at www.nature.com/reprints.

Publisher's note Springer Nature remains neutral with regard to jurisdictional claims in published maps and institutional affiliations.